Pathological Tau Induces Neurodegeneration by Sequestering and Inhibiting LSD1

Amanda K. Engstrom[1], Alicia C. Walker[1], Rohitha A. Moudgal[1], Dexter A. Myrick[1], Stephanie M. Kyle[1], David J. Katz[1*]

[1]Department of Cell Biology, Emory University School of Medicine, Atlanta GA 30322, USA.

*corresponding author:
David J. Katz
Associate Professor
Department of Cell Biology
Room 443, Whitehead Biomedical Research Building
Emory University School of Medicine
Atlanta, GA 30322, USA
Phone: (404) 727-3403
djkatz@emory.edu

Abstract

Tauopathies are a class of neurodegenerative diseases associated with pathological tau. However, the mechanism through which tau contributes to neurodegeneration remains unknown. Previously, our lab implicated the histone demethylase LSD1 in tau-induced neurodegeneration by showing that LSD1 localizes to pathological tau aggregates in Alzheimer's Disease cases, and that it is continuously required for the survival of hippocampal and cortical neurons in mice. Here, we utilize the P301S tauopathy mouse model to demonstrate that pathological tau can exclude LSD1 from the nucleus in neurons. In addition, we show that reducing LSD1 in these mice is sufficient to highly exacerbate tau-mediated neurodegeneration. Finally, we find that overexpressing LSD1 in the hippocampus of tauopathy mice, even after pathology has formed, is sufficient to significantly delay neurodegeneration. These results suggest that inhibition of LSD1 is a downstream mediator of pathological tau. Thus, LSD1 is a promising therapeutic target for tauopathies such as Alzheimer's Disease.

Introduction

Tauopathies such as corticobasal degeneration, progressive supranuclear palsy, and frontotemporal lobar degeneration with tau inclusions are neurodegenerative diseases pathologically defined by different forms of tau positive intraneuronal deposits[1-5]. In addition to these primary tauopathies, neuropathological observations of postmortem Alzheimer's Disease (AD) brains show the presence of plaques containing β-amyloid (Aβ) peptide and neurofibrillary tangles (NFTs) of hyperphosphorylated tau protein[6-9]. Thus, AD is considered a secondary tauopathy. AD is the leading cause of age-related dementia, resulting from neuronal cell death in the frontal and temporal cortices, as well as the hippocampus[7]. As dementia progresses, the

spatial pattern of tau pathology highly correlates with the level of cognitive impairment[10-13]. The most well-defined physiological role of tau is in stabilizing microtubules, particularly in neuronal axons[2]. However, in the pathological state, tau becomes aberrantly phosphorylated[2,14,15], truncated[1,4], and aggregates into oligomers and larger insoluble filaments[16,17]. These pathologies are thought to trigger synaptic loss, dramatic genome-wide expression changes, increased inflammatory response, and neuronal cell death[18-21]. In AD, Aβ plaque accumulation precedes the formation of pathological tau[6]. In addition, Aβ oligomers and/or plaques can enhance tau pathology in various mouse models[22,23], and there is increasing evidence that accumulation of Aβ plaques can contribute to tau pathology[3,24,25]. These data suggest that pathological tau may be a downstream mediator of the neurotoxic effects leading to neuronal degeneration in AD.

Previously, our lab demonstrated that deleting the histone demethylase *Lsd1* in adult mice leads to significant neuronal cell death in the hippocampus and cortex with associated learning and memory defects[26]. In this mouse model, loss of *Lsd1* induces genome-wide expression changes that significantly overlap with those observed in the brains of AD cases. Additionally, we observed LSD1 protein mislocalized to cytoplasmic NFTs[26]. These data highlight the requirement for LSD1 in neuronal survival and suggest that the nuclear function of the histone demethylase LSD1 could be disrupted by pathological tau.

To investigate how LSD1 may contribute to tau-mediated neurodegeneration, we utilized the PS19 P301S tauopathy mouse model (hereafter referred to as PS19 Tau). PS19 Tau mice express a P301S mutated form of the human tau protein, originally identified in a frontotemporal dementia with parkinsonism (FTDP-17) patient, driven by the prion promoter throughout the nervous system[27]. When expressed in mice, the P301S tau protein is prone to hyperphosphorylation and somatodendritic aggregation, without the presence of Aβ plaques.

PS19 Tau mice develop a heavy pathological tau burden and have been well characterized for the temporal progression of tau pathology and disease-related phenotypes[28,29]. However, the mechanism of neuronal cell death caused by pathological tau is still unknown.

Here, we provide functional data that the inhibition of LSD1 mediates tau induced neurodegeneration. We demonstrate in PS19 Tau mice that pathological tau sequesters LSD1 in the cytoplasm of neurons throughout the brain. This results in depletion of LSD1 from the nucleus. Additionally, we provide genetic and molecular evidence that pathological tau functions through LSD1 to induce neurodegeneration. Finally, we show that overexpressing LSD1 in hippocampal neurons is sufficient to suppress neuronal cell death even after pathological tau has formed. We propose that pathological tau leads to neuronal cell death by sequestering LSD1 in the cytoplasm, depleting the nuclear pool of LSD1 that is required for neuronal survival.

Results

Tau pathology depletes LSD1 from the nucleus in the PS19 Tau mouse model

Previously, we showed in human AD cases that LSD1 protein inappropriately colocalizes with NFTs in the cell body of hippocampal and cortical neurons, while in unaffected controls LSD1 was properly localized exclusively to the nucleus[26]. However, because neurons in AD cases with intracellular NFTs presumably die and are cleared, it was difficult to determine whether tau prevents LSD1 from localizing to the nucleus in a dying neuron. To address this possibility, we performed LSD1 immunofluorescence on 12 month old PS19 Tau mice, which have significant tau pathology[27]. Because PS19 Tau mice undergo neurodegeneration over a shortened period, there are more neurons undergoing neurodegeneration at any given time point. Thus, we reasoned that it may be possible to observe LSD1 depletion from the nucleus. Similar to what we

observe in humans, LSD1 protein in 12 month old Wild Type mice was localized to the nucleus of neurons in the hippocampus (Fig. 1a-c) and cerebral cortex (Fig. 1d-f). However, in 12 month old PS19 Tau mice, with substantial tau pathology (Fig. 1g-l), LSD1 protein was sequestered in the cytoplasm and depleted from the nucleus of neurons in the hippocampus (Fig. 1m-o) and the cerebral cortex (Fig. 1p-r). This mislocalization of LSD1 in the cytoplasm overlapped with somatodendritic pathological tau (Fig. 1s-v). Similarly, in other brain regions that accumulate tau pathology, such as the thalamus and amygdala, LSD1 was localized to the nucleus in 12 month old Wild Type control mice (Extended Data Fig. 1a-c, d-f), but abnormally localized to the cytoplasm in PS19 Tau mouse littermates (Extended Data Fig. 1g-i, j-l). Overall, we observed sequestration of LSD1 in 6 out of 7 mice analyzed. In each of the 6 mice, there were varying levels of sequestration ranging from LSD1 found in both the nucleus and cytoplasm (Extended Data Fig. 1m-o), to depletion from the nucleus (Extended Data Fig. 1p-r).

Reduction of LSD1 increases the mouse tauopathy phenotype

If the presence of pathological tau in the cytoplasm is leading to neuronal cell death through the sequestration and nuclear depletion of LSD1, we would expect that lowering the overall levels of LSD1 would accelerate depletion and exacerbate the progression of disease. To test this, we made PS19 Tau mice heterozygous for *Lsd1* (hereafter referred to as PS19;*Lsd1*$^{\Delta/+}$, Extended Data Fig. 2a). *Lsd1* heterozygotes (hereafter referred to as *Lsd1*$^{\Delta/+}$) have a functioning copy of *Lsd1* and don't have phenotypes associated with LSD1 loss of function[30-32]. Thus, *Lsd1* heterozygozity does not completely compromise LSD1 function. Instead mice that are heterozygous for *Lsd1* are sensitized to mechanisms affecting LSD1 localization and function. Consistent with this, we observed a 30% reduction in transcript levels (Extended Data Fig. 2b)

and a 35% reduction in protein levels (Extended Data Fig. 2c,d) in *Lsd1*$^{\Delta/+}$ mice compared to their *Lsd1*$^{+/+}$ littermates. Surprisingly, PS19 Tau mice have a 20% increase in LSD1 protein levels compared to *Lsd1*$^{+/+}$ littermates. Nevertheless, consistent with the reduction in LSD1 that we observe in *Lsd1*$^{\Delta/+}$ mice, PS19;*Lsd1*$^{\Delta/+}$ mice have a similar 26% reduction in transcript levels (Extended Data Fig. 2b) and a 31% reduction in protein levels (Extended Data Fig. 2c,d) compared to PS19 Tau littermates. In addition, all genotypes were born at normal Mendelian ratios with equal male/female ratios.

As expected, *Lsd1*$^{\Delta/+}$ mice had normal survival (Fig. 2a). In contrast, PS19 Tau mice had a reduced overall survival (Fig. 2a)[27]. When one copy of *Lsd1* was removed from PS19 Tau mice, their reduced survival was significantly exacerbated (P-value = 0.0017, Fig. 2a). As expected, there was little effect on the onset of reduced viability. The initial decline in the survival of PS19;*Lsd1*$^{\Delta/+}$ mice started only slightly earlier than PS19 Tau mice, but after the appearance of pathological tau in neurons (Extended Data Fig. 6k-m)[27]. This suggests that pathological tau may have to be present before *Lsd1* heterozygosity has deleterious effects. Subsequently, PS19;*Lsd1*$^{\Delta/+}$ mice had a 14% reduction in median lifespan compared to PS19 Tau mice and reached median survival 44 days earlier then PS19 Tau mice. In addition, there was a further exacerbation of reduced lifespan as pathology became more severe. PS19;*Lsd1*$^{\Delta/+}$ mice reached the point when there was only 10% of the population remaining 83 days earlier than PS19 Tau mice, and all but one of the last 25% of PS19;*Lsd1*$^{\Delta/+}$ mice died between 11.5-13.5 months, compared to 13.5-19 months in PS19 Tau mice. As a result, 28% of PS19 Tau mice were still alive after all but one of the PS19;*Lsd1*$^{\Delta/+}$ mice had died (Fig. 2a).

PS19 Tau mice develop paralysis starting with hind limb clasping which progresses until they are unable to feed[27]. In our hands, PS19 Tau mice displayed intermittent hind limb clasping

starting at approximately 6 months of age. At 12 months, these mice had a severe clasp, but were still mobile. This is delayed compared to what was originally reported by Yoshiyama and colleagues[27]. PS19;*Lsd1*$^{\Delta/+}$ mice also displayed intermittent hind limb clasping beginning at approximately 6 months of age. However PS19;*Lsd1*$^{\Delta/+}$ mice became terminally paralyzed at a faster rate compared to PS19 Tau mouse littermates. At 12 months, when PS19 Tau mice were still mobile, PS19;*Lsd1*$^{\Delta/+}$ mice were severely paralyzed and typically terminal (Supplemental Video 1). To quantitatively assess paralysis we performed rotarod and grid performance tests. In the rotarod, we assessed the ability of the mice to stay on the rotating rod (latency to fall) (Fig. 2b), the speed of the rod at which they fall off the rotarod (rotations per minute) (Fig. 2c), and the total distance traveled (Fig. 2d). All genotypes performed the same at 6 months and 8 months (Fig. 2b-d). However, at 10 months, when PS19 Tau mice still performed normally, PS19;*Lsd1*$^{\Delta/+}$ mice had a significant deficit in mobility (P-value < 0.01, Fig. 2b,c). A deficit in PS19;*Lsd1*$^{\Delta/+}$ mice was also observed at 10 months in the total distance traveled (Fig. 2d) and in grid performance testing (Extended Data Fig. 3a), though neither were statistically significant.

To further investigate the exacerbation of paralysis we examined the spinal cord motor neurons. Healthy motor neurons from *Lsd1*$^{+/+}$ control mice express LSD1 (Extended Data Fig. 3b-d) and are classically identified by circular nuclei at the center of a large cell body. In contrast to the healthy motor neurons we observed in 12 month old PS19 Tau mice (Extended Data Fig. 3e), many of the motor neurons in PS19;*Lsd1*$^{\Delta/+}$ mice at 12 months had abnormal morphology, with the nucleus skewed to the edge of the cell body (Extended Data Fig. 3e vs. 3f) and a ballooned cell body (Extended Data Fig. 3f). Within the cell body we found aberrant hyperphosphorylated NFH (heavy chain neurofilament), which is a sign of activated neuronal stress pathways (Extended Data 3g vs. 3h)[33,34]. This abnormal morphology is highly reminiscent

of a well-established process known as chromatolysis, which is characterized by swelling of the neuronal cell body, disruption of Nissl granules, and pyknotic or shrunken nuclei abnormally skewed to the edge of the cell body [35,36]. Chromatolysis, which is linked to neuronal stress and often leads to apoptosis[36], has been observed in AD and other neurodegenerative diseases[35,37-39].

Reduction of LSD1 exacerbates PS19 Tau neurodegeneration

In addition to accelerating the paralysis phenotype, reducing the level of *Lsd1* in PS19 Tau mice exacerbated neuronal cell death in the brain. At 6 months and 8 months, we observed no difference between genotypes in the overall morphology in the hippocampus (Extended Data Fig. 4a-h) based on histological analysis. There was also no difference between $Lsd1^{+/+}$ and $Lsd1^{\Delta/+}$ mice at 10 months or 12 months (Fig. 3a,b; Extended Data Fig. 4i,j,m,n; Extended Data Fig. 5a,b,e,f,i,j,m,n). At 10 months, PS19 Tau mice had very little cell loss in the hippocampus compared to $Lsd1^{+/+}$ and $Lsd1^{\Delta/+}$ control mice (Extended Data Fig. 4i-k,m-o). In contrast, at 10 months, PS19;$Lsd1^{\Delta/+}$ mice had dramatic cell loss both in the CA1 region of the hippocampus and throughout the posterior hippocampus (Extended Data Fig. 4l,p). At 12 months, the PS19 Tau mice had a slight decrease in CA1 and CA3 neurons spanning the hippocampal pyramidal cell layer compared to $Lsd1^{+/+}$ control mice (17% and 19.4% respectively, Fig. 3a,b; Extended Data Fig. 5a-c,e-g). In comparison, PS19;$Lsd1^{\Delta/+}$ mice had a 52% and 54% decrease in the CA1 and CA3 respectively (Fig. 3a,b; Extended Data Fig. 5d,h) compared to $Lsd1^{+/+}$ control mice. This resulted in decreased overall brain size (Fig. 3c) and brain weight (Fig. 3d) in PS19;$Lsd1^{\Delta/+}$ mice compared to PS19 Tau and $Lsd1^{\Delta/+}$ mouse littermates. Additionally, at 12 months there were increased levels of cell loss in the Dentate Gyrus (Extended Data Fig. 5i-l), and throughout the posterior hippocampus (Extended Data Fig. 5m-p).

Along with the histology, we monitored the progression of neuronal cell death in the same individual over time by performing magnetic resonance imaging (MRI) at 6 months and again at 10 months (Supplemental Video 2). At 6 months, there was no sign of cell loss or ventricular dilatation in *Lsd1*$^{\Delta/+}$, PS19 Tau, or PS19;*Lsd1*$^{\Delta/+}$ mice (Fig. 3e-g). However, at 10 months the MRI showed that there was dramatic ventricular dilatation in PS19;*Lsd1*$^{\Delta/+}$ mice, as evidenced by high-intensity areas in T2- weighted imaging, with substantial hippocampal and neocortical atrophy (Fig. 3j vs. 3h, Supplemental Video 2). At this timepoint, PS19 Tau mice had some ventricular dilatation and hippocampal atrophy throughout the hippocampus (Fig. 3i), but much less than PS19;*Lsd1*$^{\Delta/+}$ mice (Fig. 3j, Supplemental Video 2. 0:51 vs. 1:00sec).

Tau pathology is not affected by change in LSD1 levels

Since LSD1 is a chromatin regulator, it is possible that reducing LSD1 protein levels affects the PS19 Tau transgene. However, we confirmed that there was no difference between PS19 Tau mice and PS19;*Lsd1*$^{\Delta/+}$ mice in the endogenous mouse *Mapt* RNA expression, nor in the human P301S MAPT transgene expression (Extended Data Fig. 6a). It is also possible that LSD1 affects tau pathology. To test this, we performed immunohistochemistry staining for a hyperphosphorylated form of tau (AT8). As expected, we did not observe any AT8 positive staining in *Lsd1*$^{\Delta/+}$ at 6, 8, or 10 months (Extended Data Fig. 6b,e,h). Additionally, we observed very little AT8 positive immunoreactivity at 6 months in both PS19 Tau or PS19;*Lsd1*$^{\Delta/+}$ mice (Extended Data Fig. 6c,d). At 8 months both PS19 Tau and PS19;*Lsd1*$^{\Delta/+}$ mice had low but consistent levels of AT8 positive immunoreactivity (Extended Data Fig. 6f,g), and by 10 months both PS19 Tau and PS19;*Lsd1*$^{\Delta/+}$ mice developed the same high level of AT8 positive tau immunoreactivity (Extended Data Fig. 6i,j). This was consistent throughout both the CA1 and

CA3 regions of the hippocampus and the cerebral cortex (Extended Data Fig. 6k-m). We also did not observe any difference between PS19 Tau mice and PS19;*Lsd1*$^{\Delta/+}$ mice when assaying PHF1 (an alternative phospho-tau antibody) immunoreactivity in the CA1 region of the hippocampus at 8 months (Extended Data Fig. 7a-c,g) and 10 months (Extended Data Fig. 7d-f,g), nor in the CA3 region of the hippocampus or the cerebral cortex at 8 and 10 months (Extended Data Fig. 7h,i).

The functional interaction between tau pathology and LSD1 inhibition is specific

To test the specificity of the functional interaction between tau pathology and LSD1, we investigated the overlap in the effected molecular pathways associated with both pathological tau and *Lsd1* heterozygosity. To address this, we performed RNA sequencing on the hippocampus of 9 month *Lsd1*$^{+/+}$, *Lsd1*$^{\Delta/+}$, PS19 Tau, and PS19;*Lsd1*$^{\Delta/+}$ littermates. As opposed to analyzing transcriptional changes at the terminal stage of disease, this time point allows us to assess molecular changes prior to the onset of neuronal cell death. This is also the time point that we observed the earliest signs of exacerbation of paralysis in PS19;*Lsd1*$^{\Delta/+}$ mice. Because of this early stage in the progression of the disease, we would not expect dramatic changes in transcription overall. Nevertheless, if tau pathology is inhibiting LSD1 function, we would expect that the genome-wide expression changes induced by tau might be exacerbated by a reduction in LSD1. The RNA-seq analysis detected 271 significant gene expression changes compared to *Lsd1*$^{+/+}$ in PS19;*Lsd1*$^{\Delta/+}$ mice, 54 significant gene expression changes compared to *Lsd1*$^{+/+}$ in PS19 Tau mice, and 4 significant gene expression changes compared to *Lsd1*$^{+/+}$ in *Lsd1*$^{\Delta/+}$ mice (Extended Data Fig. 8a-f, Supplementary Table 1). We first examined the relationship between tau-induced expression changes and the effects of *Lsd1* heterozygosity by

comparing the transcriptional changes observed in PS19 Tau mice (Extended Data Fig. 8a,b) with PS19;*Lsd1*$^{\Delta/+}$ mice (Extended Data Fig. 8c,d). In PS19 Tau mice that do not yet have significant neurodegeneration, we identified 54 genes (36 up and 18 down) that were differentially expressed (Extended Data Fig. 8b). Of these 54 genes, 50 were changed in the same direction in PS19;*Lsd1*$^{\Delta/+}$ mice (93%). In addition, amongst the 50 genes changed in the same direction, 36 (72%) had exacerbated expression in PS19;*Lsd1*$^{\Delta/+}$ mice compared to PS19 Tau mice (Fig. 4a). Based on this overlap, we further compared the genome-wide expression changes between PS19 Tau mice and PS19;*Lsd1*$^{\Delta/+}$ mice. Amongst the transcripts that were changed in both PS19 Tau mice and PS19;*Lsd1*$^{\Delta/+}$ mice compared to *Lsd1*$^{+/+}$ mice, 71% changed in the same direction (either up or down). Consistent with this overlap in gene expression, Gene Set Enrichment Analysis demonstrated that many of the same pathways are affected in both PS19 Tau mice and PS19;*Lsd1*$^{\Delta/+}$ mice (Extended Data Fig. 8g-j). However, the genes affected in both sets of mice tended to be further exacerbated in PS19;*Lsd1*$^{\Delta/+}$ mice compared to PS19 Tau mice. Amongst the 71% of genes that changed in the same direction in both PS19 Tau mice and PS19;*Lsd1*$^{\Delta/+}$ mice, 76% of these transcripts had a higher fold-change in PS19;*Lsd1*$^{\Delta/+}$ mice compared to PS19 Tau mice (Fig. 4b).

LSD1's effect on expression changes in PS19 Tau mice led us to investigate if there is any overlap between tau-induced expression changes and the effects of *Lsd1* heterozygosity on its own. *Lsd1*$^{\Delta/+}$ mice had only 4 gene expression changes observed genome-wide (Extended Data Fig. 8e,f), indicating that the partially reduced level of LSD1 expression had very little effect on transcription on its own. This is consistent with the lack of phenotype in these animals. However, when we tested the specific hypothesis that the 54 genes most significantly misregulated in PS19 Tau mice might also be differentially expressed in *Lsd1*$^{\Delta/+}$ mice, we found

a class of genes (Class I) containing 22 of the 54 genes (40%) that were differentially expressed in *Lsd1*$^{\Delta/+}$ mice (Fig. 4c). Of these 22 genes in Class I that were differentially expressed in both PS19 Tau and *Lsd1*$^{\Delta/+}$ mice, all but one were changed in the same direction (Fig. 4c). This supports the idea that, although *Lsd1* heterozygosity does not result in any neurodegenerative phenotypes or genome wide expression changes, reduction of LSD1 sensitizes neurons to some of the same changes mediated by tau pathology. The remaining 32 genes (Class II) most significantly misregulated in PS19 Tau mice were largely unaffected in *Lsd1*$^{\Delta/+}$ mice (Fig. 4d).

Overexpression of LSD1 rescues neurodegeneration in the hippocampus of PS19 Tau mice

Our data demonstrate that reduction of LSD1 protein exacerbates the tauopathy phenotype in PS19 Tau mice. Based on this, we considered the possibility that overexpression of LSD1 might counter the loss of LSD1 from the nucleus and protect against neurodegeneration in PS19 Tau mice. To address this possibility, we injected PS19 Tau mice with a neuronal specific virus (AAV-DJ driven by the synapsin promoter) expressing either the full length LSD1 protein with an N-terminal HA tag (hereafter referred to as PS19- LSD1 inj) or a control virus expressing only the HA tag (hereafter referred to as PS19- HA inj). Additionally, to control for the effects of viral injection, we injected Wild Type littermates with the HA only expressing virus (hereafter referred to as WT- HA inj). All injections were performed directly into the hippocampus at 8-8.5 months, when tau pathology is already present throughout the nervous system. Immunolabeling for the HA tag demonstrated that the virus is specific to NeuN+ neurons (Extended Data Fig. 9a-d), with no HA expression observed in IBA+ microglia (Extended Data Fig. 9e-h), or GFAP+ astrocytes (Extended Data Fig. 9i-l). It also confirmed that virally expressed LSD1 is nuclear (Extended Data Fig. 9m) and confined to the hippocampus (Extended Data Fig. 9n). After 3

months of overexpression, 11-11.5 month old mice were euthanized, and the brains were analyzed. Injections resulted in a ~6-fold increase in expression of LSD1 in the hippocampus compared to endogenous LSD1 in the PS19- HA inj mice, but no increase in the cerebellum (Extended Data Fig. 9o,p). As expected, because the viral injections were restricted to the hippocampus, the mice injected with LSD1 still developed paralysis (Supplemental Video 3). This confirms that the tau transgene is expressed and functioning. Additionally, we did not observe a difference in total levels of AT8 positive tau immunoreactivity (Extended Data Fig. 9q-t). Therefore, any modulation to the phenotype was not due to changes in tau pathology.

Injected mice were evaluated for cell death by neuronal cell counts in the hippocampus. Injection of LSD1 virus into the hippocampus of PS19 Tau mice rescued the neurodegeneration phenotype. We observed significantly more neurons (P-value <0.05) spanning the pyramidal cell layer (84% of WT- HA inj CA1 counts) compared to their PS19- HA inj littermates (59% of WT- HA inj CA1 counts), such that overall the neuronal cell count in PS19- LSD1 inj mice was not statistically different from the WT- HA inj (Fig. 5a-d). Additionally, in the histological analysis we observed a large number of cells infiltrating the hippocampus in PS19- HA inj mice compared to WT- HA inj littermates (Fig. 5b vs. 5c). Marker analysis demonstrated that this was due to a strong inflammatory response, with a large increase in the number of GFAP+ astrocytes (Extended Data Fig. 10a-c vs. d-f) and TRL2+ activated microglia (Extended Data Fig. 10j-l vs. m-o, s-v vs. w-z,ee). Injection of PS19 Tau mice with LSD1 virus rescued this inflammatory response. For example, all but one (9 out of 10 analyzed) of the PS19- LSD1 inj mice had a reduction in the number of GFAP+ astrocytes (Extended Data Fig. 10g-i vs. d-f) and TRL2+ activated microglia (Extended Data Fig. 10p-r vs. m-o, aa-dd vs. w-z, ee). Of note, the one PS19- LSD1 inj mouse where we did observe increased glial cells, similar to PS19- HA inj mice, had

the lowest neuronal cell count (74% of WT- HA inj CA1 neurons). It is possible that this mouse was already undergoing neurodegeneration prior to the injection of the LSD1 overexpression virus.

Although the number of hippocampal neurons in PS19- LSD1 inj mice did not differ from WT- HA inj controls, in 6 of the 10 PS19- LSD1 inj mice we observed cells with abnormal blebbed nuclei at varying numbers throughout the hippocampus (Fig. 5e). These abnormal cells are rare in PS19- HA inj mice, which have a reduced overall number of cells in the pyramidal cell layer compared to WT- HA inj control mice. One possibility is that these abnormal cells with blebbing nuclei represent an intermediate state between a healthy neuron and a dying neuron that is prolonged by rescue via LSD1 overexpression. Interestingly, these abnormal cells also differed in the localization of HA-tagged LSD1. The four mice with normal nuclei had HA-tagged LSD1 protein localized uniformly throughout the nucleus (Fig. 5f). In contrast, the six mice with abnormal nuclear blebbing had some HA-tagged LSD1 that was mislocalized to the cytoplasm (Fig. 5g). This includes the one PS19- LSD1 inj mouse that had an elevated number of astrocytes and TRL2 positive microglia. Thus, the blebbing state correlates with when the viral produced LSD1 begins to be sequestered in the cytoplasm, similar to the endogenously produced LSD1.

Discussion

In this study we investigate a potential downstream mediator of tau pathology in neurodegenerative disease. We find that modulation of the chromatin modifying enzyme LSD1 can alter neurodegeneration in a tauopathy mouse model. Previously, we showed that LSD1 colocalizes with tau pathology in the cell body of neurons in AD cases[26]. This suggested that

LSD1 might be disrupted in tauopathies such as AD, by being excluded from the nucleus. To address this directly, we utilize the PS19 tauopathy mouse model. In these mice, we find that LSD1 is sequestered in the cytoplasm, in some cases being completely depleted from the nucleus. This provides the first cytological evidence that pathological tau can prevent LSD1 from properly localizing to the nucleus in hippocampal and cortical neurons, where we have previously shown it is continuously required.

Based on the ability of pathological tau to sequester LSD1, we hypothesized that neuronal cell death may be due, at least partly, to LSD1 being sequestered in the cytoplasm and depleted from the nucleus. In this case, reducing LSD1 levels should make it easier for tau to deplete LSD1 from the nucleus, resulting in a faster progression of neurodegeneration and/or a more severe neurodegenerative phenotype. Importantly, LSD1 heterozygosity alone does not lead to any neurodegeneration. This suggests that any effects observed in PS19;*Lsd1*$^{\Delta/+}$ mice are not simply due to LSD1 haploinsufficiency. Normally, PS19 Tau mice develop paralysis and neurodegeneration, along with reduced survival. In contrast, when we reduce LSD1 in the PS19 Tau mice, PS19;*Lsd1*$^{\Delta/+}$ mice die significantly earlier, most likely due to the increased rate of paralysis. Additionally, PS19;*Lsd1*$^{\Delta/+}$ mice have increased neuronal cell death and clearance in the hippocampus. This suggests that pathological tau functions through LSD1 to cause neurodegeneration *in vivo* in mice.

PS19;*Lsd1*$^{\Delta/+}$ mice have a 31% reduction in LSD1 protein levels compared to PS19 Tau mice from birth. This reduction should theoretically make mice sensitive to LSD1 depletion at any time. However, tau pathology starts at 6-8 months in PS19 Tau mice. As a result, if *Lsd1* heterozygosity is functioning by making it easier for pathological tau to deplete LSD1 from the nucleus, we would not expect to see any exacerbation until after pathological tau is present. The

exacerbation of the PS19 Tau mouse neurodegenerative phenotype does not occur until after pathological human tau was present. This suggests that the effect of *Lsd1* heterozygosity requires the presence of pathological tau, placing LSD1 downstream of tau. Consistent with LSD1 being downstream of pathological tau, we found no evidence that *Lsd1* heterozygosity affects the expression of the tau transgene, or the buildup of pathological tau in PS19 Tau mice.

To test whether the functional interaction between pathological tau and reduced LSD1 is specific, we used RNA-seq to determine whether the downstream molecular pathways altered in PS19 Tau mice are exacerbated in PS19;$Lsd1^{\Delta/+}$ mice. This analysis was performed at the time of earliest signs of neuronal distress, allowing us to assess molecular changes prior to cell death and clearance. Surprisingly, some of the genes altered in PS19 Tau mice are also affected in *Lsd1* heterozygous mice, which do not have a neurodegenerative phenotype. This suggests that despite having no association with neurodegenerative disease, reduction of LSD1 by 35% compared to Wild Type already primes some genes for tau-mediated neurodegeneration. Moreover, when LSD1 is reduced in PS19 Tau mice, the genome-wide expression changes induced by pathological tau are specifically exacerbated. Taken together, these results suggest that the functional interaction that we observe between pathological tau and reduced LSD1 is occurring through the tau pathway.

Our previous data implicated LSD1 in the tau-mediated neurodegeneration pathway. Utilizing the PS19 Tau mouse model, we now show a functional interaction between pathological tau and LSD1. Importantly, because PS19 Tau mice do not have Aβ plaque accumulation, this functional interaction is specific to tau. Based on these data we propose the following model (Supplementary Video 4): in healthy hippocampal and cortical neurons, LSD1 is translated in the cytoplasm and transported into the nucleus where it is continuously required

to repress inappropriate transcription. In tauopathy, pathological tau accumulates in the cytoplasm blocking LSD1 from nuclear import. This interferes with the continuous requirement for LSD1, resulting in neuronal cell death. Recently, it has been observed that the nuclear pore breaks down in AD[40-42]. It should be noted that this mechanism would potentially exacerbate the model that we propose.

This model makes a direct prediction: if tau is predominantly functioning through LSD1, then increasing the levels of LSD1 should rescue the tau-induced neurodegenerative phenotype. To address this, we overexpressed LSD1 in the hippocampal neurons of PS19 Tau mice. Overexpression of LSD1 specifically in hippocampal neurons rescues the neuronal cell death and limits the inflammatory response. This rescue is neuronal specific, suggesting that the functional interaction between LSD1 and tau is occurring in neurons. In addition, this rescue occurs despite there being no effect on tau aggregation. This negates the possibility that the tau transgene is simply not functioning when LSD1 is overexpressed. The ability of LSD1 overexpression to overcome tau-mediated neurodegeneration in the presence of pathological tau aggregates, provides further evidence that pathological tau is functioning through the inhibition of LSD1. Importantly, overexpressing LSD1 should not prevent it from being sequestered. Rather overexpressing LSD1 should make it more difficult for pathological tau to sequester all of the LSD1 protein, allowing some LSD1 to be transported to the nucleus. Thus, overexpressing LSD1 would be expected to temporarily rescue the ability of pathological tau to kill neurons. Consistent with this, LSD1 overexpression delays the effect of pathological tau rather than permanently rescuing. In 60% of the mice, the surviving neurons have abnormal morphology, and the overexpressed version of LSD1 is also sequestered. observation that neurons fail to maintain their morphology when the overexpressed LSD1 begins to be sequestered in the

cytoplasm provides further support for the model that tau mediates neurodegeneration through the sequestration of LSD1. Nevertheless, our data suggest that overexpression of LSD1 cannot permanently overcome pathological tau. To permanently overcome pathological tau, it would likely be necessary to permanently disrupt the interaction between pathological tau and LSD1. This work is currently ongoing in the lab. Overall, our data establish LSD1 as a major downstream effector of tau-mediated neurodegeneration. Based on these data, we propose that the LSD1 pathway is a potential late stage target for intervention in tauopathies, such as AD.

Methods

All mouse work, including surgical procedures, were approved by and conducted in accordance with the Emory University Institutional Animal Care and Use Committee.

Mouse tissue fixation

Mice were given a lethal dose of isoflurane via inhalation, then transcardially perfused with ice cold 4.0% paraformaldehyde in 0.1M phosphate buffer. Brain and spinal cord were dissected and post fixed in cold paraformaldehyde solution for 2 hours. Brain weights and sizes were taken from mice that were euthanized by cervical dislocation. Brain was dissected, immediately weighed, imaged, and fixed in cold 4.0% paraformaldehyde in 0.1M phosphate buffer overnight. In all cases, tissues were transferred to cold PBS, then serially dehydrated and embedded in paraffin and serially sectioned into 20µm coronal sections.

Histology and histological studies

Hematoxylin and eosin staining was performed according to standard procedures. Briefly, sections were dewaxed with xylenes and serial ethanol dilutions then stained with Eosin using the Richard-Allan Scientific Signature Series Eosin-Y package (ThermoScientific). To derive

unbiased estimates of neuronal loss in the hippocampus, the number of primordial neurons in CA1 and CA3 (corresponding approximately to bregma coordinates -2.0 mm and -3.0 mm) were counted from 2 randomly selected regions in the field of a Zeiss Axiophot ocular graticule grid and measured manually using digital micrographs of H&E-stained preparations. Investigators were blinded to the genotype or treatment.

Immunohistochemistry and immunofluorescence

Sections were dewaxed with xylenes and serial ethanol dilutions, then treated with 3% hydrogen peroxide at 40°C for 5 minutes to quench endogenous peroxidase activity, blocked in 2% serum at 40°C for 15 minutes, and incubated with primary Ab (Supplementary Table 2) overnight at 4°C. Slides were washed, then incubated with biotinylated secondary Ab (Biotinylated Goat α Rabbit, 1:200, Vector Labs BA-1000 or Biotinylated Goat α Mouse, 1:200, Vector Labs BA-9200) at 37°C for 30 minutes. Signal amplification was then carried out by incubating at 37°C for 1 hour with Vector Labs Elite ABC reagent (PK-6200). Slides were developed with DAB for 1-5 minutes, counterstained with hematoxylin for 1 minutes, and coverslipped. For immunofluorescence, dewaxed sections were first rinsed with TBS. Antigen retrieval was performed by microwaving at 10% power 2X for 5 minutes in 0.01M sodium citrate. Slides were then cooled, washed with TBS, permeabilized in 0.5% Triton X-100 for 20 minutes, followed by blocking in 10% goat serum 20 minutes. Primary Abs (Supplementary Table 2) were incubated overnight at 4°C. Slides were then washed and incubated in secondary Abs (Invitrogen A1 1001 and Invitrogen A11012) for 1 hour at room temperature, followed by TBS washes, counterstained with DAPI, and then coverslipped. For the assessment of tau accumulation, six random sections (sampling from CA1, CA3, and cerebral cortex) per sample were manually

counted using digital micrographs of AT8 stained preparations in the field of a Zeiss Axiophot ocular graticule grid. Investigators were blinded to the genotype or treatment.

Protein Quantification

Protein levels were determined by homogenizing brains in 1 ml/g of tissue in ice-cold lysis buffer (150mM NaCl, 1% Triton X-100, 0.5% Na-deoxycholate, 1% SDS, 50mM Tris, pH8.0) in a dounce homogenizer, followed by end-over-end spin at 4°C for 2 hours, and centrifugation at 20,000 x g for 20 minutes at 4°C. Protein concentrations were determined following standard BCA protocol (Pierce BCA Protein Assay Kit). Equal amounts of protein for each sample were loaded and run on a 12% SDS-PAGE gel, transferred (Semi-dry transfer using BIO RAD Trans-Blot Turbo Transfer System), blocked in 5% BSA, and probed with primary Ab (Supplementary Table 2) over night at 4°C. Blots were rinsed and stained with HRP-conjugated secondary Ab, and detected by chemiluminescence using ChemiDoc MP Imaging System (BIO RAD). Protein levels were normalized using total protein calculated using BIO RAD ImageLab software.

Quantitative analysis of paralysis

We performed experiments on PS19 Tau, *Lsd1*$^{\Delta/+}$, PS19;*Lsd1*$^{\Delta/+}$ mice at 6, 8, and 10 months. For the rotarod experiments, mice were given two practice trials and then placed on the rotating cylinder at 4rpm. Rotational speed then gradually increased over a 5-minute test session up to a maximum rotational speed of 40rpm. Latency to fall off of the accelerating rotarod was used as the dependent variable. We calculated the latency to fall, maximum speed in rotations per minute, and distance traveled. For grid performance, mice were placed on a horizontal grid that was then inverted so mice are hanging upside down by their paws. Mice were videotaped for 10 seconds, and then scored for forepaw and back paw distance traveled. Mice that could not hold

onto grid for 10 seconds were censored. Investigators were blinded to the genotypes for both experiments.

MRI of brain atrophy

MRI studies were conducted on PS19 Tau, *Lsd1*$^{\Delta/+}$, PS19;*Lsd1*$^{\Delta/+}$ mice at 6 months and 10 months (*n*=3/genotype). Mice were anesthetized with isoflurane, and monitored for heart rate and temperature changes while anesthetized. MRI measurements were performed using a 9.4 T/20 cm horizontal bore Bruker magnet, interfaced to an AVANCE console (Bruker, Billerica, MA, USA). A two-coil actively decoupled imaging set-up was used (a 2 cm diameter surface coil for reception and a 7.2 cm diameter volume coil for transmission). Axial T2-weighted images were acquired with a RARE (Rapid Acquisition with Refocused Echos) sequence. Its imaging parameters were as follows: TR = 3000 ms, Eff.TE = 64 ms, RARE factor = 4, field of view (FOV) = 23.04 × 23.04 mm2, matrix = 192 × 192, Avg = 4, slice thickness (thk) = 0.6 mm, number of slice(NSL)=20. Specific emphasis was placed on the neocortex and hippocampus in the coronal images (1.0 – 4.0 mm posterior to the bregma).

RNA sequencing

9 month old *Lsd1*$^{+/+}$, *Lsd1*$^{\Delta/+}$, PS19 Tau, and PS19;*Lsd1*$^{\Delta/+}$ littermates (n=2 mice/genotype) were euthanized by cervical dislocation, hippocampi were dissected and snap frozen with liquid nitrogen in 1mL Trizol, and stored at -80°C. For RNA isolation, samples were thawed at 37°C then kept on ice prior to homogenization with Polytron homogenizer with a 5 second pulse. After a 5 minute incubation at room temperature, one tenth the sample volume of 1-bromo-3chloropropane was added, mixed by inversion and incubated for 3 minutes at room temperature. Samples were then centrifuged at 13,000 X g for 15 minutes at 4°C to separate the aqueous and organic layers. As much of the aqueous layer was recovered as possible, then RNA was

precipitated with isoproponal. Pellets were then washed with 75% ethanol and resuspended in 50µL of dionized water. RNA library preparation and sequencing were performed by HudsonAlpha Genomic Services Lab. RNA was Poly(A) selected and 300bp size selected. Libraries were sequenced for 25 million 50bp paired end reads.

RNA sequencing analysis

The sequencing data were uploaded to the Galaxy web platform, and *we used the public server at* usegalaxy.org *to analyze the data*[43,44]. FASTQ files were quality assessed using FASTQC (v.0.11.7), trimmed using Trimmomatic (v.0.36.5) and minimum QC score of 20 and minimum read length of 36bp. Paired-end reads were subsequently mapped to the GRCm38 genome using HISAT2 (v.2.1.0). Unmapped, unpaired and multiply mapped reads were removed using Filter SAM or BAM (v.1.1.2). Assignment of transcripts to GRCm38 genomic features was performed using Featurecounts (v.1.6.0.6) and the Ensembl GRCm38.93 gtf file. Differentially expressed transcripts were determined using DESEQ2 (v.2.11.40.2)[44]. For all datasets, a cutoff of adjusted p-value < 0.3 and abs ($\log_2$ fold change) > 0.58 was applied. TPM values were calculated from raw data obtained from Featurecounts output. Subsequent downstream analysis was performed using R and normalized counts and adjusted P-values from DESEQ2 (v.2.11.40.2). Heatmaps were produced and hierarchical clustering was done using the gplots package (v. 3.0.1) and normalized counts[45]. Volcano plots were produced using the enhanced volcano package (v.0.99.16) and adjusted p-values[46]. Additionally, Gene Set Enrichment Analysis (Pre-ranked list) was performed using the online platform WebGestalt[47-50]. Custom R-scripts available upon request.

Stereotaxic surgery and viral infusion

All surgical procedures were approved by and conducted in accordance with the Emory University Institutional Animal Care and Use Committee. Mice were anesthetized with isoflurane (3% induction, 1-2% maintenance) and administered the analgesic meloxicam (5 mg/kg). Using a Stoeling Quintessential Stereotaxic Injector pump and Hamilton syringe, mice were injected with either the AAV-DJ-LSD1- HA virus or the control AAV-DJ- HA virus into both hippocampi. Each virus was injected into the rostral (AP: -2.5, ML:± 2.2, DV: -1.6, relative to bregma) and caudal (AP: -3.1, ML:± 3.0, DV: -3.5) hippocampus of both hemispheres (four injection sites total). Infusion volumes were 0.5 µL per injection site, administered at a rate of 0.15 µL/min. Following surgery, mice were monitored daily for the duration of the experiment. Brains were extracted 3 months post-surgery which allows sufficient time for viral expression. Injection accuracy was confirmed by HA positive staining, and those mice where staining was outside the hippocampus or that did not fully reach hippocampus were censored.

Data availability

FastQ files for the RNA sequencing experiments are bring deposited in the GEO and will be available upon publication. Results from DESEQ2 are available in Supplementary Table 1

Supplementary Information is linked to the online version of the paper at www.nature.com/nature.

Acknowledgments

We thank M. Rosenfeld (U.C.S.D) for providing *Lsd1* deletion mice; N. Seyfried, R. Betarbet, Mr. Gearing, from the Emory ADRC (P50 AG025688), NINDS Emory Neuroscience Core Facilities (P30NS055077) for tissue processing and providing PHF1 antibody, J. Alcudia of the

Stanford Gene Vector and Virus Core for the help with virus generation and production; J. Schroeder from Emory Rodent Behavioral Core for help with Rotatord and Grid Performance assays supported by the Emory Neuroscience NINDS Core Facilities (P30NS055077) with further support provided by the Georgia Clinical & Translational Science Alliance of the National Institutes of Health under Award Number UL1TR002378; and J. Park from the Emory Center for Systems Imagining for preforming MRI supported by the National Center for Advancing Translational Sciences of the National Institutes of Health under Award Number UL1TR000454. We would also like to thank M.J. Rowley and V. Corces for assistance on RNA sequencing analysis, K.Porter-Stransky and D. Weinshenker for providing PS19 Tau mouse and teaching stereotaxic surgery procedure; D. Weinshenker, A. Levey, C. Bean and T. Caspary for comments on the manuscript and assistance throughout. Additionally the authors would like to thank fellow Katz lab members for assistance experimentally and intellectually. A.K.E was supported by the National Institute of General Medicine training grant (T32 GM008367-26) and an NRSA from National Institute of Neurological Disorders and Stroke (NINDS) (F31 NS098663-02). D.A.M was supported by a research supplement to promote diversity in health-related research from the NINDS (1R01NS087142). S.M.K was supported the NINDS Training in Translational Research in Neurology grant (5T32 NS007480-17). The work was supported by a grant to D.J.K from the National Institute of Neurological Disorders and Stroke (1R01NS087142).

Author Contributions A.K.E and D.J.K. conceived and designed the study and wrote the manuscript. A.K.E. performed experiments with the help of A.C.W, S.M.K, and R.A.M under the direction of D.J.K. D.A.M performed bioinformatics analysis on the RNA sequencing data.

A.K.E, A.C.W, S.M.K, and R.A.M analyzed all other data and interpreted results. All authors discussed the results and commented on the manuscript.

Author Information Reprints and permissions information are available at www.nature.com/reprints. The authors declare no competing financial interests. Correspondence and requests for materials should be addressed to D.J.K. (djkatz@emory.edu).

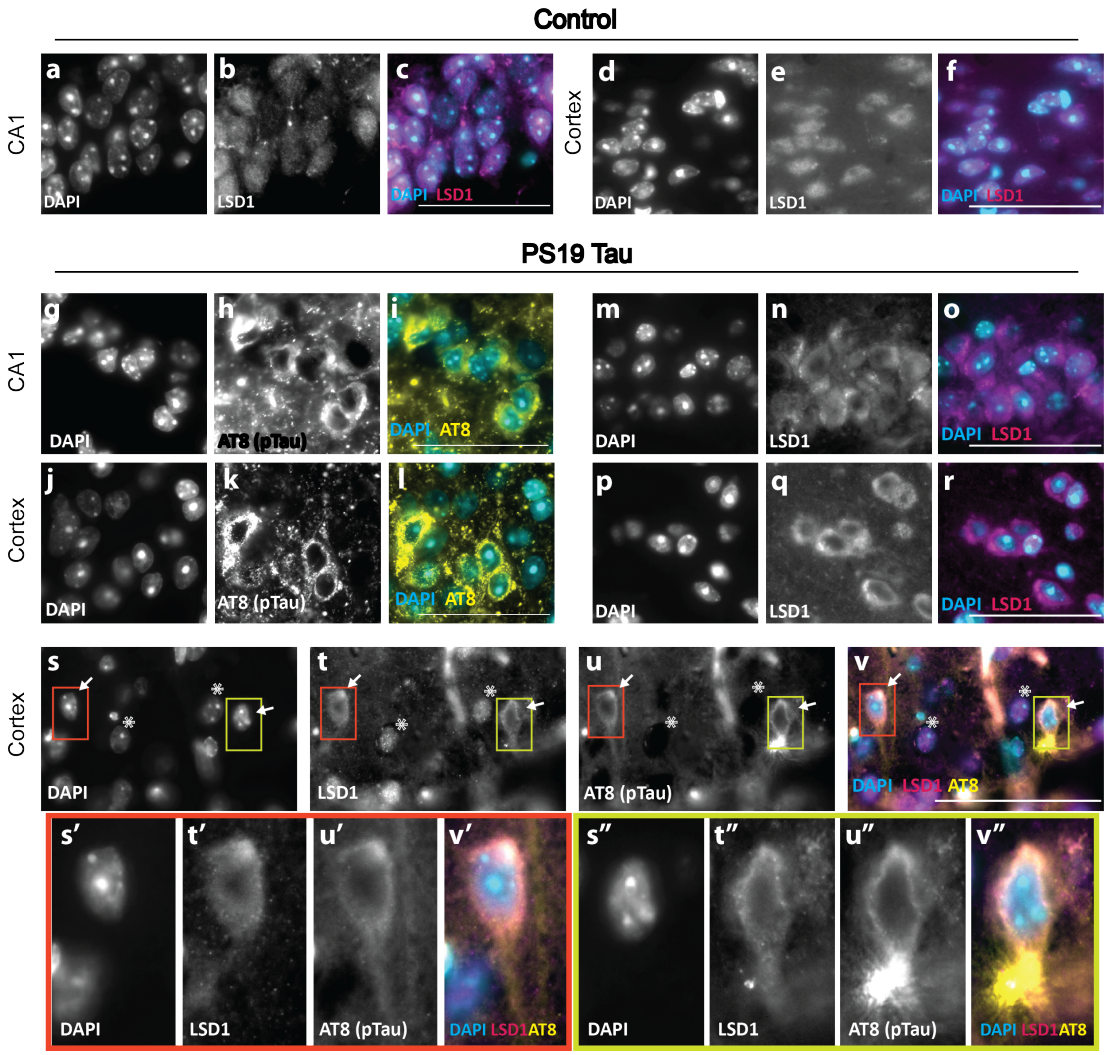

Fig. 1: LSD1 localizes to pathological tau and is sequestered in the cytoplasm. a-f, Representative immunofluorescence of 12 month old control Wild Type mice showing DAPI (**a,d**), LSD1 (**b,e**), and merged (**c,f**) in the CA1 region of the hippocampus (**a-c**) and the cerebral cortex (**d-f**). LSD1 is localized specifically to DAPI positive nuclei. **g-l**, Representative immunofluorescence showing DAPI (**g,j**), AT8 positive hyper-phosphorylated tau (**h,k**), and merged (**i,l**) in the CA1 region of the hippocampus (**g-i**) and the cerebral cortex (**j-l**) of 12 month old PS19 Tau mice. Hyper-phosphorylated tau accumulates in cell bodies. **m-r**, Representative immunofluorescence showing DAPI (**m,p**), LSD1 (**n,q**), and merged (**o,r**) in 12 month old PS19 Tau mice. LSD1 is localized outside, and depleted from, the nucleus in the CA1 region of the hippocampus (**m-o**) and the cerebral cortex (**p-r**). **s-v,** Representative immunofluorescence showing DAPI (**s**), LSD1 (**t**), AT8 (**u**), and merge (**v**). Arrows denote cells where LSD1 is localized to extra-nuclear hyperphosphorylated pathological tau. Asterisks denote LSD1 localized specifically to the nucleus of cells without hyperphosphorylated tau. The corresponding channels of the cells boxed in red and yellow are shown magnified in **s'-v'** and **s''- v''** respectively. *n*=7 mice analyzed (images representative of 6 of the 7 mice analyzed). Scale bars=50μm.

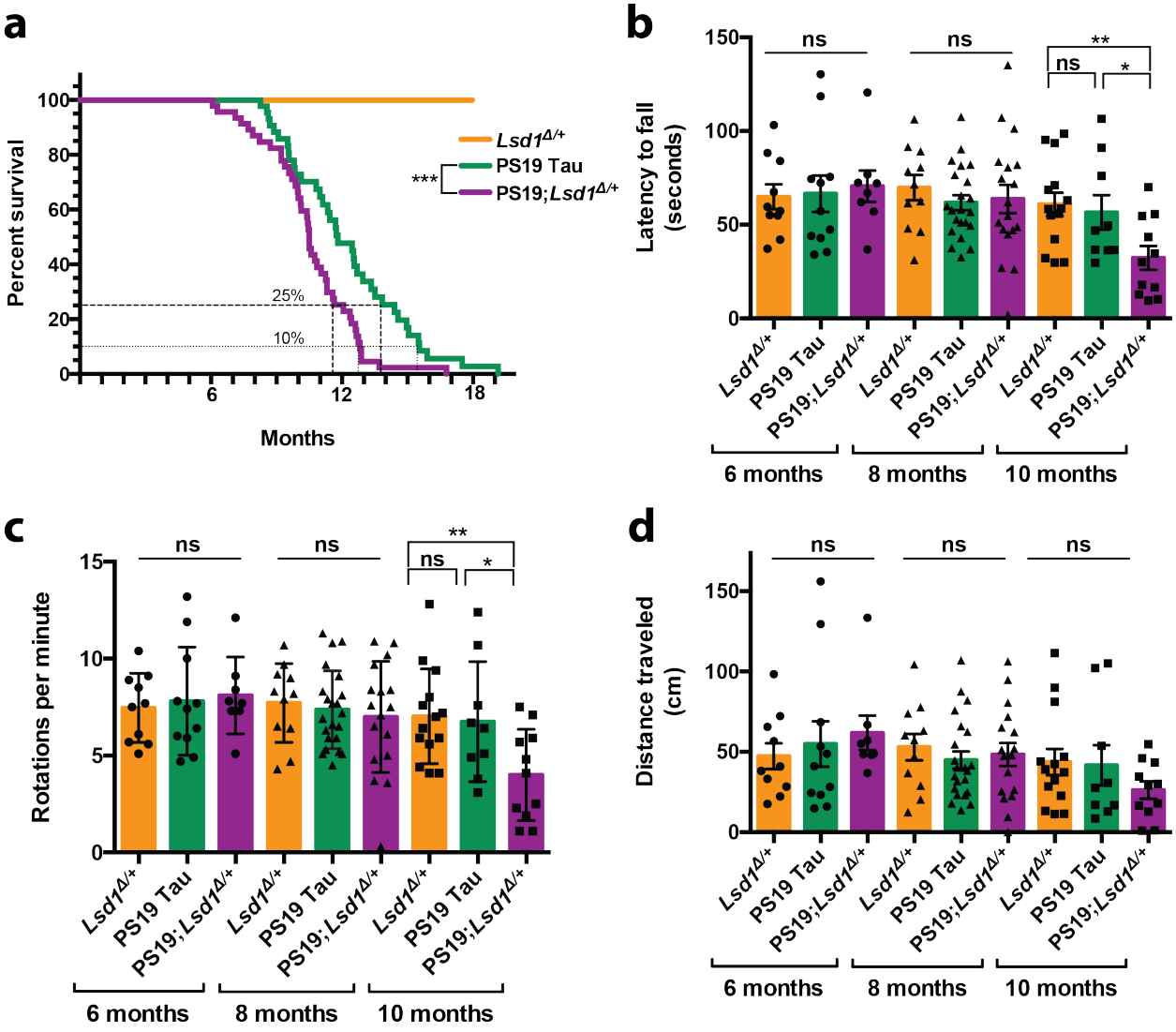

Fig. 2: Reduction of *Lsd1* exacerbates the PS19 Tau mouse paralysis phenotype. a, Lifespan curve showing that no $Lsd1^{\Delta/+}$ mice died before 18 months (orange, *n*=20). PS19;$Lsd1^{\Delta/+}$ mice (purple, *n*=44) have a significant reduction in survival compared to PS19 Tau mice with wild-type levels of *Lsd1* (green, *n*=37)(Log-rank Mantle-Cox test ***P<0.005). **b-d**, Rotarod testing of latency to fall (in seconds) (**b**), rotations per minute (when the mouse fell) (**c**), and distance traveled (in centimeters) (**d**) for mice at age 6, 8 and 10 months. $Lsd1^{\Delta/+}$ (orange, *n*=10,11,14), PS19 Tau (green, *n*=11,22,9), and PS19;$Lsd1^{\Delta/+}$ (purple, *n*=8,17,11). Values are mean ± SEM (two-way analysis of variance (ANOVA) with Tukey's post hoc test *P<0.05 **P<0.01, ns=not significant).

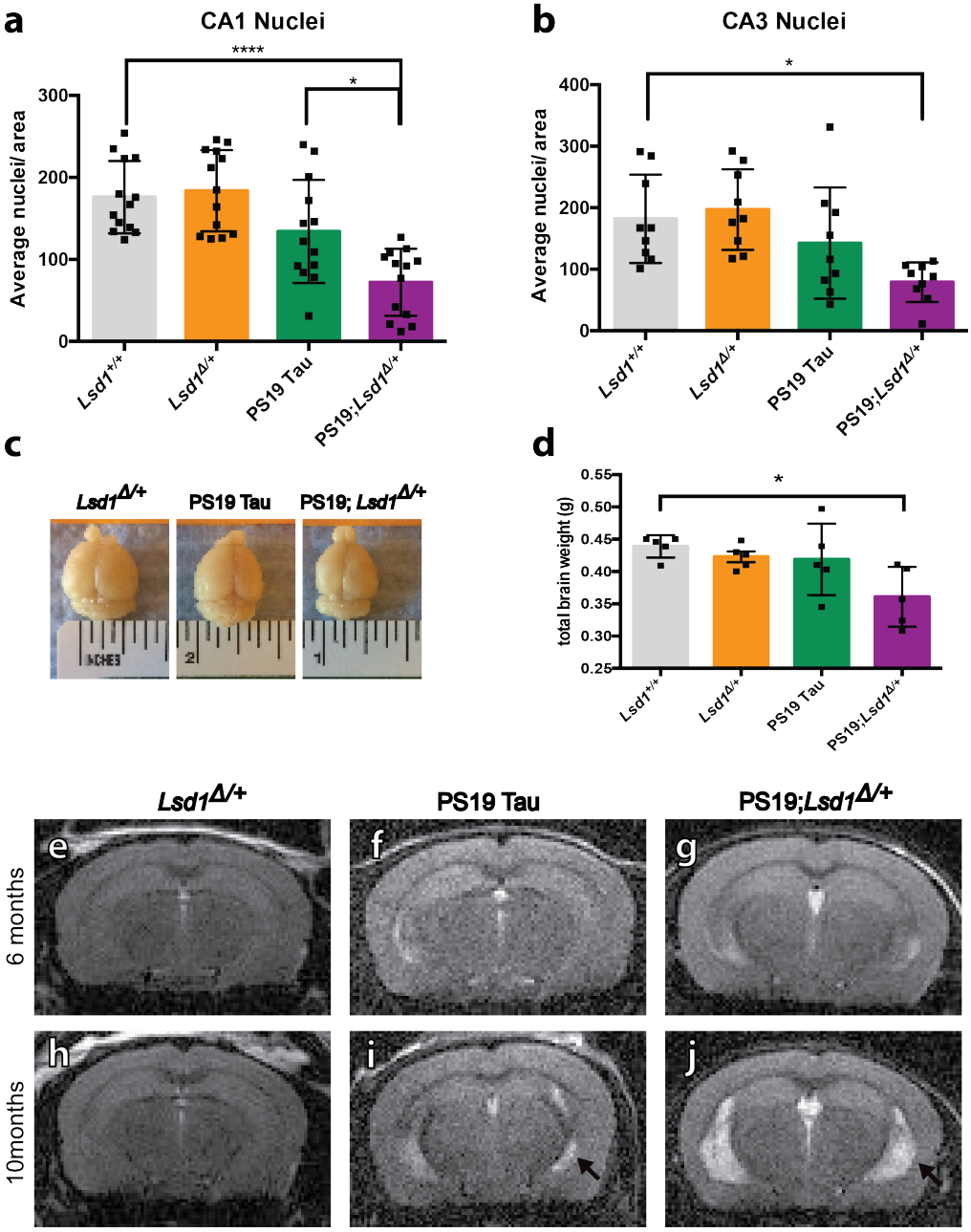

Fig. 3: Reduction of *Lsd1* exacerbates neurodegeneration in PS19 Tau mice. a,b, Average nuclei per area in the CA1 (**a**) and CA3 (**b**) regions of the hippocampus in 12 month old $Lsd1^{+/+}$, $Lsd1^{\Delta/+}$, PS19 Tau, and PS19;$Lsd1^{\Delta/+}$ mice. Quantification from histology represented in **Extended Data Fig. 5a-h**. Values are mean ± SD (**a**, *n*=13 & **b,** *n*=9). **c,** Representative image of the brains of 12 month old $Lsd1^{\Delta/+}$, PS19 Tau, and PS19;$Lsd1^{\Delta/+}$ littermates. **d,** Total brain weight of 12 month old littermates represented in **Fig. 3c.** Values are mean ± SD (*n*=5). For all graphs: one-way analysis of variance (ANOVA) with Tukey's post hoc test (two-sided) *P<0.05,****P<0.001. **e-j,** Representative image of T2- weighted RARE coronal MRI taken from 6 months (**e-g**) and 10 months (**h-j**) of age in $Lsd1^{\Delta/+}$ (**e,h**), PS19 (**f,i**), and PS19;$Lsd1^{\Delta/+}$ (**g,j**) mice (*n*=3). Arrow denotes region of hippocampal atrophy.

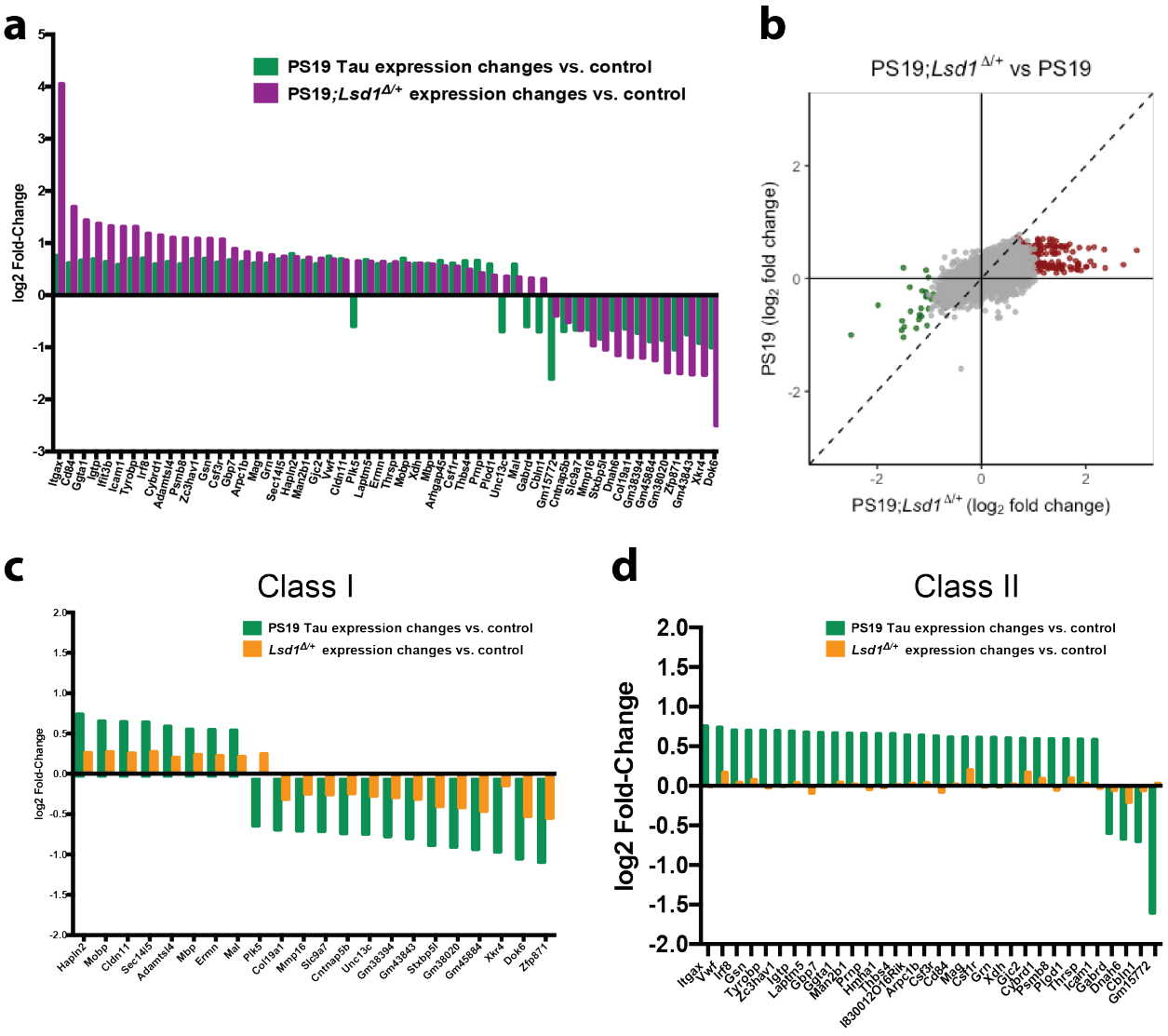

Fig. 4: Molecular overlap between loss of LSD1 function and tauopathy. a, Histogram (log_2 fold change) of the 54 genes that have significant changes in expression in the PS19 Tau mouse (green) and their expression changes in the PS19;*Lsd1*$^{\Delta/+}$ mouse (purple). **b,** Scatter plot showing the correlation between the genome-wide log_2 fold change in gene expression between PS19 Tau and PS19;*Lsd1*$^{\Delta/+}$. The most significantly changed genes in PS19;*Lsd1*$^{\Delta/+}$ mouse are shown in red (upregulated) and green (downregulated). All other genes are shown in grey. Dotted line represents 1:1 relationship between gene expression changes in PS19 Tau vs. PS19;*Lsd1*$^{\Delta/+}$. Genes with correlated expression changes are found in the top right and bottom left quadrants, while genes that do not correlate are found in the opposite quadrants. **c**, Histogram showing the log_2 fold change of the Class I genes (22 of the 54 genes differentially expressed in PS19 Tau) in PS19 Tau (green) and *Lsd1*$^{\Delta/+}$ (orange). **d,** Histogram showing the log_2 fold change of the Class II genes (32 of the 54 genes differentially expressed in PS19 Tau) in PS19 Tau (green) and *Lsd1*$^{\Delta/+}$ (orange).

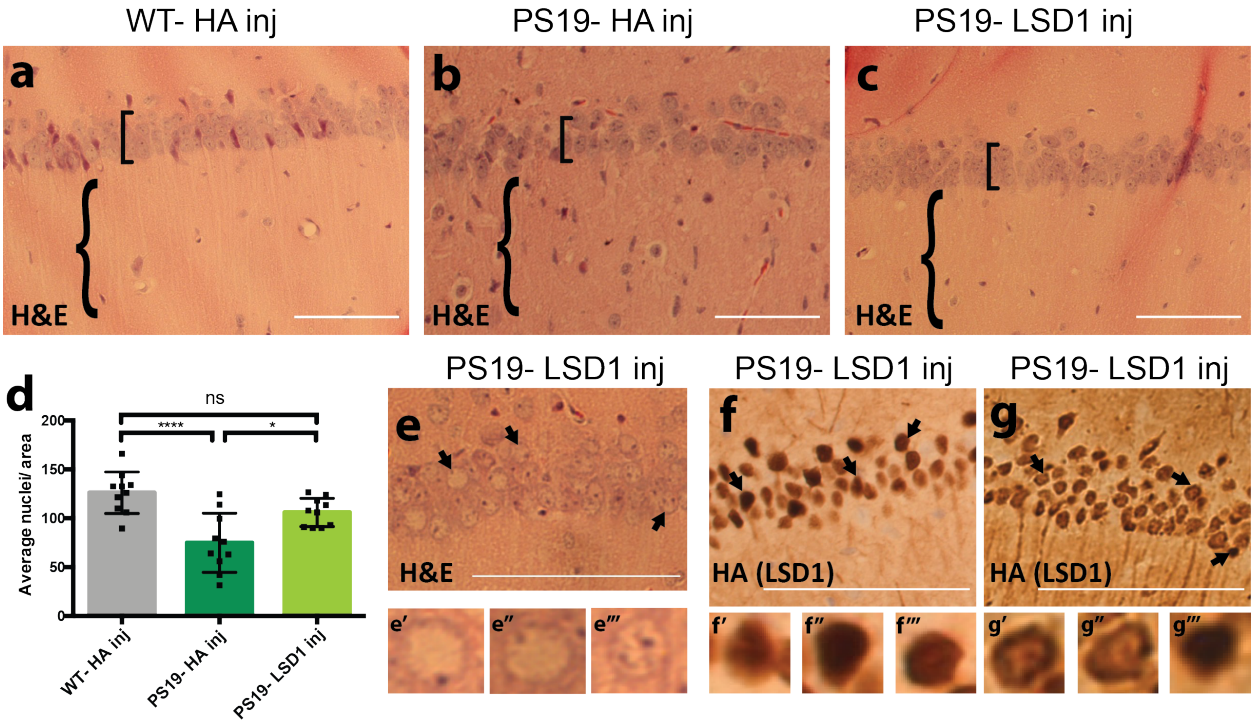

Fig. 5: LSD1 overexpression reduces the neurodegenerative phenotype in 11 month old PS19 Tau mice. a-c, Representative image of H&E stained CA1 region of the hippocampus of 11 month old Wild Type mice injected with HA control virus (WT- HA inj) (**a**), PS19 Tau mice injected with HA control virus (PS19- HA inj) (**b**), and PS19 Tau mice injected with *Lsd1* overexpressing virus (PS19- LSD1 inj) (**c**). Square brackets denote thickness of pyramidal layer of the CA1 of the hippocampus and curvy brackets denote hippocampal region with or without infiltrating cells. **d,** Quantification of the average number of nuclei in the pyramidal layer of the hippocampus per area per mouse from histology represented in **Fig. 5a-c**. Values are mean ± SD (n=10, one-way analysis of variance (ANOVA) with Tukey's post hoc test, *p<0.05, ****p<0.001, ns=not significant). **e,** Representative H&E of PS19- LSD1 inj mouse with abnormal nuclei blebbing in the CA1 region of the hippocampus. **e'-e''',** High magnified image of cells denoted by arrows in **Fig. 5e** of individual nuclei that are either abnormally blebbed (**e', e"**) or normal (**e'''**). **f,g,** Immunohistochemistry staining of HA(LSD1) in 11 month PS19- LSD1 inj mice. HA is either localized specifically to the nucleus in all nuclei (**f**) or in only a few nuclei while it is partially sequestered in the cytoplasm in others (**g**). **f'-f''',** High magnified image of cells denoted by arrows in **Fig. 5f** of nuclear HA localization in individual nuclei. **g'-g''',** High magnified image of cells denoted by arrows in **Fig. 5g** of individual nuclei with HA(LSD1) either sequestered to the cytoplasm (**g', g"**) or confined to the nucleus (**g'''**). Scale bars=50µm.

1 Orr, M. E., Sullivan, A. C. & Frost, B. A Brief Overview of Tauopathy: Causes, Consequences, and Therapeutic Strategies. *Trends in pharmacological sciences* **38**, 637-648, doi:10.1016/j.tips.2017.03.011 (2017).

2 Wang, Y. & Mandelkow, E. Tau in physiology and pathology. *Nat Rev Neurosci* **17**, 5-21, doi:10.1038/nrn.2015.1 (2016).

3 Holtzman, D. M. *et al.* Tau: From research to clinical development. *Alzheimers Dement* **12**, 1033-1039, doi:10.1016/j.jalz.2016.03.018 (2016).

4 Wischik, C. M. *et al.* Isolation of a fragment of tau derived from the core of the paired helical filament of Alzheimer disease. *Proc Natl Acad Sci U S A* **85**, 4506-4510, doi:10.1073/pnas.85.12.4506 (1988).

5 Goedert, M., Wischik, C. M., Crowther, R. A., Walker, J. E. & Klug, A. Cloning and sequencing of the cDNA encoding a core protein of the paired helical filament of Alzheimer disease: identification as the microtubule-associated protein tau. *Proc Natl Acad Sci U S A* **85**, 4051-4055, doi:10.1073/pnas.85.11.4051 (1988).

6 Hardy, J. & Selkoe, D. J. The amyloid hypothesis of Alzheimer's disease: progress and problems on the road to therapeutics. *Science* **297**, 353-356, doi:10.1126/science.1072994 (2002).

7 Barage, S. H. & Sonawane, K. D. Amyloid cascade hypothesis: Pathogenesis and therapeutic strategies in Alzheimer's disease. *Neuropeptides* **52**, 1-18, doi:10.1016/j.npep.2015.06.008.

8 Bloom, G. S. Amyloid-β and Tau: The Trigger and Bullet in Alzheimer Disease PathogenesisAmyloid-β and TauAmyloid-β and Tau. *JAMA Neurology* **71**, 505-508, doi:10.1001/jamaneurol.2013.5847 (2014).

9 Duyckaerts, C., Delatour, B. & Potier, M.-C. Classification and basic pathology of Alzheimer disease. *Acta Neuropathologica* **118**, 5-36, doi:10.1007/s00401-009-0532-1 (2009).

10 Arriagada, P. V., Growdon, J. H., Hedley-Whyte, E. T. & Hyman, B. T. Neurofibrillary tangles but not senile plaques parallel duration and severity of Alzheimer's disease. *Neurology* **42**, 631-639, doi:10.1212/wnl.42.3.631 (1992).

11 Karran, E., Mercken, M. & De Strooper, B. The amyloid cascade hypothesis for Alzheimer's disease: an appraisal for the development of therapeutics. *Nat Rev Drug Discov* **10**, 698-712, doi:10.1038/nrd3505 (2011).

12 Gomez-Isla, T. *et al.* Neuronal loss correlates with but exceeds neurofibrillary tangles in Alzheimer's disease. *Ann Neurol* **41**, 17-24, doi:10.1002/ana.410410106 (1997).

13 Bejanin, A. *et al.* Tau pathology and neurodegeneration contribute to cognitive impairment in Alzheimer's disease. *Brain* **140**, 3286-3300, doi:10.1093/brain/awx243 (2017).

14 Hanger, D. P., Betts, J. C., Loviny, T. L., Blackstock, W. P. & Anderton, B. H. New phosphorylation sites identified in hyperphosphorylated tau (paired helical filament-tau) from Alzheimer's disease brain using nanoelectrospray mass spectrometry. *J Neurochem* **71**, 2465-2476, doi:10.1046/j.1471-4159.1998.71062465.x (1998).

15 Morishima-Kawashima, M. *et al.* Hyperphosphorylation of tau in PHF. *Neurobiol Aging* **16**, 365-371; discussion 371-380 (1995).

16 Arendt, T., Stieler, J. T. & Holzer, M. Tau and tauopathies. *Brain Research Bulletin* **126**, 238-292, doi:https://doi.org/10.1016/j.brainresbull.2016.08.018 (2016).

17 Castellani, R. J. & Perry, G. Tau Biology, Tauopathy, Traumatic Brain Injury, and Diagnostic Challenges. *J Alzheimers Dis* **67**, 447-467, doi:10.3233/jad-180721 (2019).

18 Masliah, E. *et al.* Altered expression of synaptic proteins occurs early during progression of Alzheimer's disease. *Neurology* **56**, 127-129, doi:10.1212/wnl.56.1.127 (2001).

19 Ingelsson, M. *et al.* Early Abeta accumulation and progressive synaptic loss, gliosis, and tangle formation in AD brain. *Neurology* **62**, 925-931, doi:10.1212/01.wnl.0000115115.98960.37 (2004).

20 Kinney, J. W. *et al.* Inflammation as a central mechanism in Alzheimer's disease. *Alzheimer's & Dementia: Translational Research & Clinical Interventions* **4**, 575-590, doi:https://doi.org/10.1016/j.trci.2018.06.014 (2018).

21 Rubio-Perez, J. M. & Morillas-Ruiz, J. M. A review: inflammatory process in Alzheimer's disease, role of cytokines. *TheScientificWorldJournal* **2012**, 756357-756357, doi:10.1100/2012/756357 (2012).

22 Hurtado, D. E. *et al.* A{beta} accelerates the spatiotemporal progression of tau pathology and augments tau amyloidosis in an Alzheimer mouse model. *Am J Pathol* **177**, 1977-1988, doi:10.2353/ajpath.2010.100346 (2010).

23 He, Z. *et al.* Amyloid-beta plaques enhance Alzheimer's brain tau-seeded pathologies by facilitating neuritic plaque tau aggregation. *Nat Med* **24**, 29-38, doi:10.1038/nm.4443 (2018).

24 Choi, S. H. *et al.* A three-dimensional human neural cell culture model of Alzheimer/'s disease. *Nature* **515**, 274-278, doi:10.1038/nature13800 http://www.nature.com/nature/journal/v515/n7526/abs/nature13800.html#supplementary-information (2014).

25 Braak, H. & Braak, E. Frequency of Stages of Alzheimer-Related Lesions in Different Age Categories. *Neurobiology of Aging* **18**, 351-357, doi:https://doi.org/10.1016/S0197-4580(97)00056-0 (1997).

26 Christopher, M. A. *et al.* LSD1 protects against hippocampal and cortical neurodegeneration. *Nature Communications* **8**, 805, doi:10.1038/s41467-017-00922-9 (2017).

27 Yoshiyama, Y. *et al.* Synapse Loss and Microglial Activation Precede Tangles in a P301S Tauopathy Mouse Model. *Neuron* **53**, 337-351, doi:10.1016/j.neuron.2007.01.010.

28 Bellucci, A. *et al.* Induction of Inflammatory Mediators and Microglial Activation in Mice Transgenic for Mutant Human P301S Tau Protein. *The American Journal of Pathology* **165**, 1643-1652, doi:http://dx.doi.org/10.1016/S0002-9440(10)63421-9 (2004).

29 Iba, M. *et al.* Tau pathology spread in PS19 tau transgenic mice following locus coeruleus (LC) injections of synthetic tau fibrils is determined by the LC's afferent and efferent connections. *Acta Neuropathol* **130**, 349-362, doi:10.1007/s00401-015-1458-4 (2015).

30 Foster, C. T. *et al.* Lysine-specific demethylase 1 regulates the embryonic transcriptome and CoREST stability. *Molecular and cellular biology* **30**, 4851-4863, doi:10.1128/MCB.00521-10 (2010).

31 Jin, L. *et al.* Loss of LSD1 (lysine-specific demethylase 1) suppresses growth and alters gene expression of human colon cancer cells in a p53- and DNMT1(DNA methyltransferase 1)-independent manner. *The Biochemical journal* **449**, 459-468, doi:10.1042/BJ20121360 (2013).

32 Lyons, D. B. *et al.* An epigenetic trap stabilizes singular olfactory receptor expression. *Cell* **154**, 325-336, doi:10.1016/j.cell.2013.06.039 (2013).
33 Giasson, B. I. & Mushynski, W. E. Aberrant stress-induced phosphorylation of perikaryal neurofilaments. *J Biol Chem* **271**, 30404-30409, doi:10.1074/jbc.271.48.30404 (1996).
34 Liu, Y. L. *et al.* Alternation of neurofilaments in immune-mediated injury of spinal cord motor neurons. *Spinal Cord* **47**, 166, doi:10.1038/sc.2008.90 (2008).
35 Moon, L. D. F. Chromatolysis: Do injured axons regenerate poorly when ribonucleases attack rough endoplasmic reticulum, ribosomes and RNA? *Dev Neurobiol* **78**, 1011-1024, doi:10.1002/dneu.22625 (2018).
36 Cragg, B. G. What is the signal for chromatolysis? *Brain Res* **23**, 1-21, doi:10.1016/0006-8993(70)90345-8 (1970).
37 Sil, S., Goswami, A. R., Dutta, G. & Ghosh, T. Effects of naproxen on immune responses in a colchicine-induced rat model of Alzheimer's disease. *Neuroimmunomodulation* **21**, 304-321, doi:10.1159/000357735 (2014).
38 Riancho, J. *et al.* Compensatory Motor Neuron Response to Chromatolysis in the Murine hSOD1(G93A) Model of Amyotrophic Lateral Sclerosis. *Front Cell Neurosci* **8**, 346, doi:10.3389/fncel.2014.00346 (2014).
39 Cataldo, A. M., Hamilton, D. J. & Nixon, R. A. Lysosomal abnormalities in degenerating neurons link neuronal compromise to senile plaque development in Alzheimer disease. *Brain Res* **640**, 68-80, doi:10.1016/0006-8993(94)91858-9 (1994).
40 Eftekharzadeh, B. *et al.* Tau Protein Disrupts Nucleocytoplasmic Transport in Alzheimer's Disease. *Neuron* **99**, 925-940.e927, doi:https://doi.org/10.1016/j.neuron.2018.07.039 (2018).
41 Sheffield, L. G., Miskiewicz, H. B., Tannenbaum, L. B. & Mirra, S. S. Nuclear Pore Complex Proteins in Alzheimer Disease. *Journal of Neuropathology & Experimental Neurology* **65**, 45-54, doi:10.1097/01.jnen.0000195939.40410.08 (2006).
42 Frost, B., Bardai, F. H. & Feany, M. B. Lamin Dysfunction Mediates Neurodegeneration in Tauopathies. *Curr Biol* **26**, 129-136, doi:10.1016/j.cub.2015.11.039 (2016).
43 Afgan, E. *et al.* The Galaxy platform for accessible, reproducible and collaborative biomedical analyses: 2016 update. *Nucleic Acids Res* **44**, W3-w10, doi:10.1093/nar/gkw343 (2016).
44 Afgan, E. *et al.* The Galaxy platform for accessible, reproducible and collaborative biomedical analyses: 2018 update. *Nucleic Acids Research* **46**, W537-W544, doi:10.1093/nar/gky379 (2018).
45 Gregory R. Warens, B. B., Lodewijk Bonebakker, Robert Gentleman, Wolfgang Huber Andy Liaw, Thomas Lumley, Martin Maechler, Arni Magnusson, Steffen Moeller, Marc Schwartz, Bill Venables. *gplots: Various R Programming Tools for Plotting Data versiou 3.0.1.1.*, < https://CRAN.R-project.org/package=gplots> (2019).
46 Blighe, K. *EnhancedVolcano: Publication-ready volcano plotswith enhanced colouring and labeling.*, <https://github.com/kevinblighe/EnhancedVolcano> (2019).
47 Wang, J., Duncan, D., Shi, Z. & Zhang, B. WEB-based GEne SeT AnaLysis Toolkit (WebGestalt): update 2013. *Nucleic Acids Res* **41**, W77-83, doi:10.1093/nar/gkt439 (2013).
48 Wang, J., Vasaikar, S., Shi, Z., Greer, M. & Zhang, B. WebGestalt 2017: a more comprehensive, powerful, flexible and interactive gene set enrichment analysis toolkit. *Nucleic Acids Res* **45**, W130-w137, doi:10.1093/nar/gkx356 (2017).

49 Liao, Y., Wang, J., Jaehnig, E. J., Shi, Z. & Zhang, B. WebGestalt 2019: gene set analysis toolkit with revamped UIs and APIs. *Nucleic Acids Res* **47**, W199-w205, doi:10.1093/nar/gkz401 (2019).

50 Zhang, B., Kirov, S. & Snoddy, J. WebGestalt: an integrated system for exploring gene sets in various biological contexts. *Nucleic Acids Res* **33**, W741-748, doi:10.1093/nar/gki475 (2005).